DOI 10.1007/s11182-020-02124-1
*Russian Physics Journal, Vol. 63, No. 6, October, 2020 (Russian Original No. 6, June, 2020)*

# DEFECT FORMATION IN TITANIUM ALLOY DURING NON-STATIONARY PROCESS OF LOCAL METALLURGY

**K. N. Kalashnikov, A. V. Chumaevskii, T. A. Kalashnikova, K. S. Osipovich, and E. A. Kolubaev**

UDC 658.5.012.1

*The paper studies* Ti-6Al-4V *alloy specimens obtained by wire-based electron-beam additive manufacturing (EBAM) and characterized by the structure with a defective region produced by uncontrolled wire fluctuations during 3D printing. Metallographic analysis and tensile strength tests and microhardness measurements are conducted to determine the defect influence on the structure and properties of the alloy. It is shown that the defective region represents the primary β-phase grains that are finer than those of the EBAM specimens commonly exhibiting a columnar structure. The specimen microhardness both in the defective and defect-free regions, is identical. The deformation behavior of the alloy is mostly subject to the influence of such defects, since the plasticity and ultimate tensile strength of the defective region are respectively higher and lower than that of the defect-free region.*

**Keywords**: additive manufacturing technology, titanium alloy, mechanical properties, microstructure.

## INTRODUCTION

Additive manufacturing technologies have been recently of great interest both for manufacturers and researchers. For manufacturers in various industries, additive manufacturing technologies can make a huge leap forward in reducing the lead time and eco-friendly manufacturing of parts for various applications. For example, in additive manufacturing of high-pressure titanium spherical cylinders, the material consumption can be reduced through minimization of the processing and mechanical operations. The advantages of additive manufacturing technologies make them ideal to replace traditional production methods. There are a number of such technologies that differ in the feedstock feeding and heat sources that provide its melting [1]. Based on these criteria, additive manufacturing technologies can be classified by 1) the source type, namely laser, electron-beam, arc, plasma, *etc*. [2–5] and 2) the feedstock, which is usually powder or wire [6, 7]. This work focuses on the wire-based electron-beam additive manufacturing (EBAM) characterized by the non-stationary process of local metallurgy, which occurs during the material layer deposition.

Wire-based additive manufacturing using an electron beam as a heat source is successful in manufacturing large-sized products from different metals and alloys [8–10], including titanium [11, 12]. According to [13], wire-based EBAM is widely used in manufacturing of high-pressure titanium spherical cylinders, carriers and other parts for aviation and aerospace applications. Moreover, Wanjara, *et al*. [14] show the possibility of using EBAM in repair and recovery of damaged parts of aircraft engines. Owing to rather a wide applicability of this method, the study of the manufacturing process of products from different materials is a highly topical task for many researchers around the world. There is however little information in the literature about the EBAM geometrical parameters and stability. It is

Institute of Strength Physics and Materials Science of the Siberian Branch of the Russian Academy of Sciences, Tomsk, Russia, e-mail: kkn@ispms.tsc.ru; tch7av@gmail.com; gelombang@ispms.tsc.ru; osipovich_k@ispms.tsc.ru; eak@ispms.tsc.ru. Translated from Izvestiya Vysshikh Uchebnykh Zavedenii, Fizika, No. 6, pp. 57–62, June, 2020. Original article submitted February 12, 2020.

 

TABLE 1. EBAM Parameters for Ti-6Al-4V Alloy Specimens

| Accelerating voltage, kV | Current intensity, mA | Linear printing speed, mm/min | E-beam profile, mm |
|---|---|---|---|
| 30.0 | 31.5 | 220.0 | 5.0 |

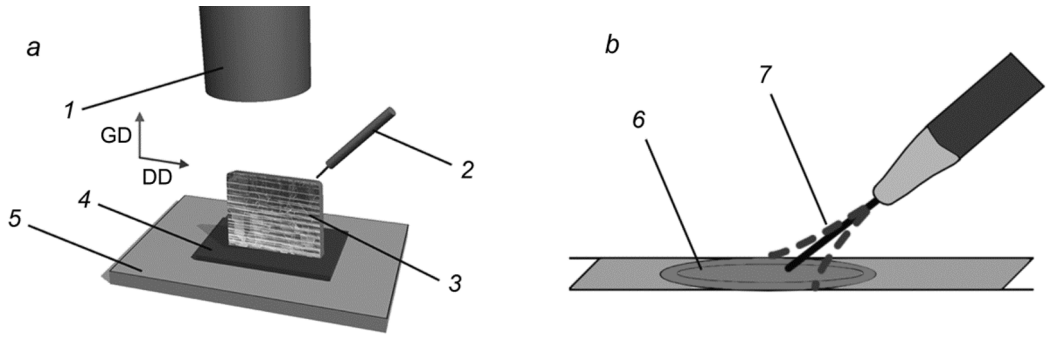


Fig. 1. Schematic representation of wire-feed electron beam additive manufacturing (*a*) and wire fluctuations (*b*): *1* – EB gun, *2* – wire feeder, *3* – printed object (vertical wall), *4* – substrate, *5* – thee axis table, *6* – melted pool, *7* – wire fluctuations, DD – deposition direction, GD – growth direction.

known that these factors may directly affect the structure and properties of the final product [15, 16]. For example, Wu, *et al.* [16] demonstrate how the printing path affects the fabrication of vertical walls made from titanium alloy in using wire arc additive manufacturing. The stability of the printing process can be determined by many factors. In this work, the stability of wire feeding is used as the stability criterion, to be more precise, the wire fluctuations, which can occur uncontrollably due to the specific design of the printing system. The wire fluctuations may be caused by an inaccurate arrangement of the wire feeder, small radius of the wire coil, and others. The purpose of this work is to study the structure and mechanical properties of the vertical wall specimens produced by the printing process accompanied by uncontrolled wire fluctuations.

## MATERIALS AND METHODS

In this work, we studied the EBAM specimens of the Ti-6Al-4V alloy obtained in the form of vertical walls using the test equipment developed at the Institute of Strength Physics and Materials Science SB RAS, Tomsk, Russia. The Ti-6Al-4V alloy wire with a diameter of 1 mm was used as the feedstock. A 2.5 mm thick substrate was made of commercial titanium VT1-0 (Grade 2) and placed onto a steel plate with a 5 mm thickness. The schematic of wire-feed electron beam additive manufacturing and wire fluctuations are given in Fig. 1.

Table 1 presents the EBAM parameters for the Ti-6Al-4V alloy specimens. It should be noted that in this table, the current intensity of the electron beam is average, while in the 3D printing process, it is successively changed from 35.0 mA for the first layers to 28.0 mA for the upper layers. In order to provide the formation of the melted pool comparable with the required wall width, we use a circular e-beam profile.

Using electric discharge machining, dog bone and metallographic specimens were cut from the EBAM vertical walls to conduct the tensile strength tests and metallographic measurements, respectively. This is illustrated in Fig. 2.

The surface structure was investigated using an Altami MET 1C metallographic microscope (Russia) after its polishing by abrasive machining with the different sandpaper grit, diamond polishing paste with a soft tissue and then chemical etching for 40 seconds in Kroll's reagent. The microhardness testing was performed on a Duramin 5 (Denmark) hardness tester at a 100 g indentation load. Static tension tests of the dog bone specimens were carried out on a universal testing machine UTS-110M-100 (Russia). The dog bone specimen cutting was performed along and

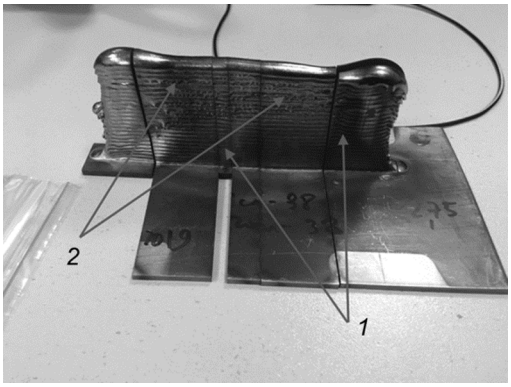


Fig. 2. Photograph of electric discharge machining: *1* – metallographic specimen fabrication, *2* – dog bone specimen fabrication.

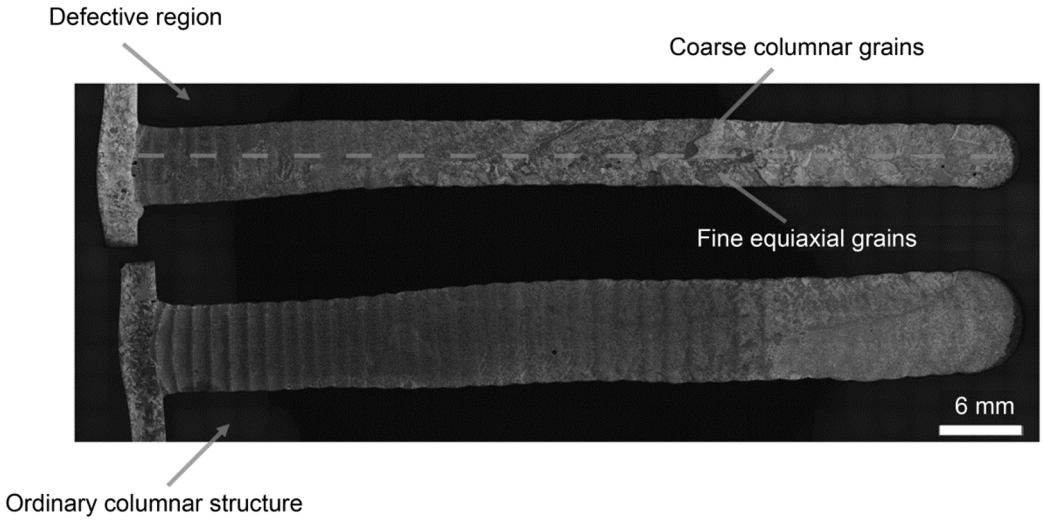


Fig. 3. Metallographic images of the Ti-6Al-4V alloy microstructure and the defective region along the vertical wall.

crosswise of the deposition direction. These specimens had a 23 mm length, 12 mm length and 2.5 mm width of the working part, and 2 mm thickness. The X-ray diffraction (XRD) analysis of the phase composition was carried out by DRON-7 diffractometer (Burevestnik, Russia).

## RESULTS AND DISCUSSION

As expected, the specimens obtained at the wire fluctuations demonstrate the structure with of a macrodefect, namely an extended defective region. According to the metallographic analysis, the defective region of the wall is characterized by a decrease in its thickness to 4.0 mm, the thickness of the defect-free region being 6–7 mm. This factor may be decisive in the case of operation of a product with such a defect, since usually the product geometry must possess a certain dimension tolerance for subsequent machining, which will be discussed later.

As can be seen from Fig. 3, the defect-free regions of the specimen comprise the primary β-phase columnar grains and the lamellar α-phase grains. The former penetrates along the vertical axis, in the direction of the wall growth. One grain can grow through tens of successively deposited layers. Thus, during solidification, the non-stationary

TABLE 2. XRD Results of Defective Region of Ti-6Al-4V Alloy Specimen

| Top specimen part | | Bottom specimen part | |
|---|---|---|---|
| α′ + β | | α + β | |
| α′ | β | α | β |
| $a$ = 2.93196, $c$ = 4.67850, $c/a$ = 1.59569 | $a$ = 3.30210 | $a$ = 2.92754, $c$ = 4.68772, $c/a$ = 1.60125 | $a$ = 3.27706 |

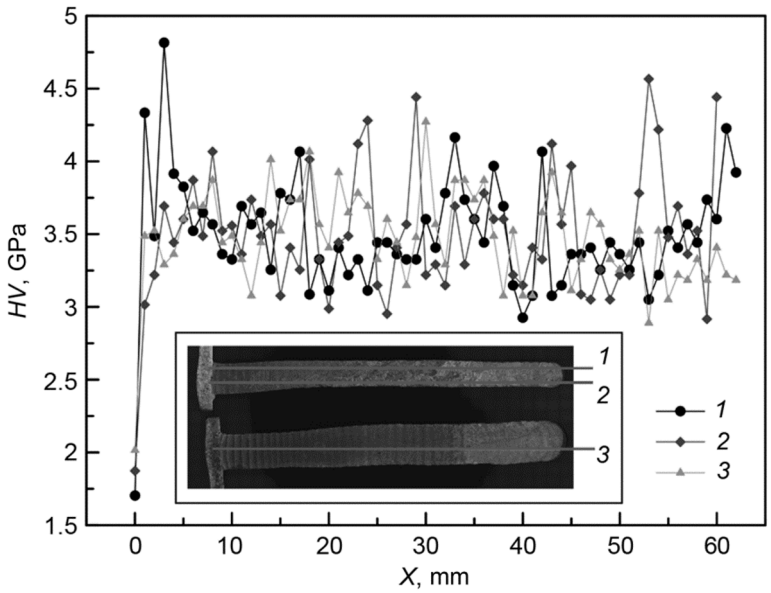


Fig. 4. Microhardness distribution along the wall height: *1* – columnar grain, *2* – equiaxial grain, *3* – defect-free regions.

process of local metallurgy of the Ti-6Al-4V alloy is characterized by the epitaxial grain growth. As for the defective region, only partial formation of such a structure is observed.

In Fig. 3, the defective region can be conventionally divided into two parts, namely: with refined equiaxial grains generated by the wire fluctuations and without the latter, but having the typical columnar grains. It is interesting that this structure prevails throughout the wall height, starting from the first layer. The primary β-phase grain size in the defective region is 1.1 ± 0.3 mm, whereas in the defect-free region it is 9.75 ± 4.43 mm long and 2.25 ± 0.41 mm wide. This is probably because the wire mechanical processing during the layer deposition, since the temperature conditions remain unchanged. And the primary β-phase columnar grain size is 15.42 ± 11.79 mm long and 3.34 ± 1.37 mm wide.

The XRD results are summarized in Table 2. One can see that the phase composition in the defective region is similar both in the top and bottom specimen parts. In both cases, α- and residue β-phase are present. Nevertheless, the lattice parameters are different in these phases. According to Lia, *et al*. [17], the degree of tetragonality ($c/a$) of the α-phase lattice shows that α-phase in the top part is α′-phase. Such a phase composition correlates with our previous research [15], which however demonstrates the α′-phase presence in the bottom part also. In addition, the presence of residue β-phase in the top part is likely to be caused by the decrease in the grain size and, consequently, the volume fraction of the primary grain boundaries. Nevertheless, the phase distribution along the wall height is quite common and does not significantly change due to the presence of the defective region, which will be confirmed by mechanical testing of the specimens.

In order to understand how the structure obtained during the non-stationary process of local metallurgy in the defective region affects the mechanical properties of the alloy specimen, the microhardness was measured on the surface of metallographic specimens. The measurement results are shown in Fig. 4.

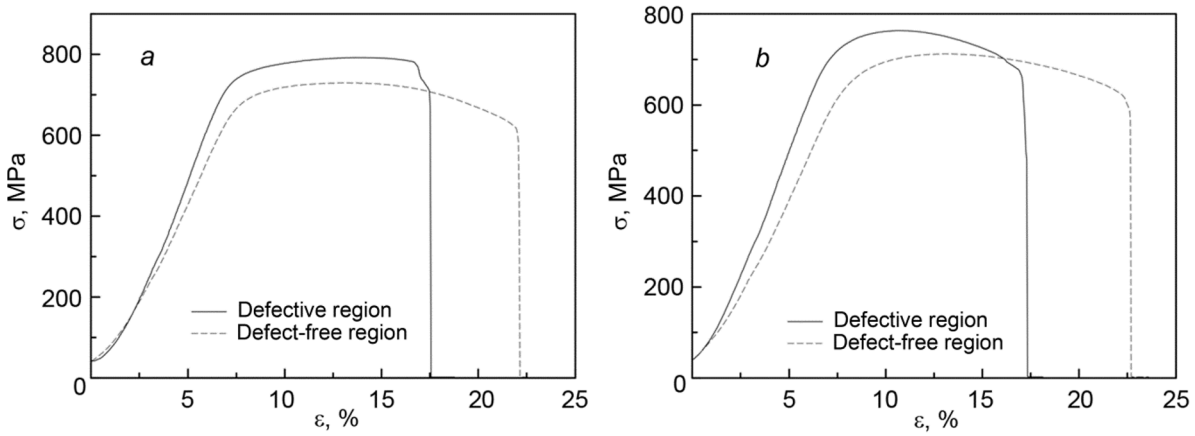


Fig. 5. Stress-strain curves of dog bone specimens cut along (*a*) and crosswise (*b*) of the deposition direction.

As Fig. 4 shows, the structure and phase transformations in the defective region do not cause changes in the alloy microhardness, despite the increase in the grain size of the β-phase. In each of the three cases, the microhardness corresponds to the as-cast Ti-6Al-4V alloy hardness. Thus, for the defective region, the average microhardness of the columnar structure (Curve 1) is 3.50 ± 0.25 GPa, and that of the equiaxial grain structure (Curve 2) is 3.52 ± 0.28 GPa. The microhardness of the defect-free region (Curve 3) is 3.52 ± 0.32 GPa. Thus, the obtained values change within the margin of error. Therefore, it can be concluded that the change in the grain size of the primary β-phase does not affect the Ti-6Al-4V alloy microhardness. Apparently, the main contribution to the measured parameter makes α-phase rather than β-phase, since the temperature conditions during the printing process remain unchanged, and the α-phase lamellar structure is identical both in the defective and defect-free regions.

In spite of this, static tension tests of the dog bone specimens show that the detected macrodefect influences the deformation behavior of the material.

Figure 5 contains the stress-strain curves obtained after the tensile strength tests. According to this figure, the material has different values of the ultimate tensile strength (UTS) and elongation in the defective and defect-free regions both in the deposition and the growth directions. Thus, in each of the directions, the defective region has the higher UTS, namely 792 MPa in the longitudinal and 764 MPa in the crosswise direction. The UTS in the defect-free region is 729 and 712 MPa for the longitudinal and crosswise directions, respectively. In both directions, the relative elongation is 12 and 16% in the defective and defect-free regions, respectively.

Based on the results, it can be concluded that the alloy structure modified by the defective region changes the deformation behavior during static tension of the material. The reduction in the initial grain size results in the increased UTS and decreased plasticity. Bermingham, *et al*. [18] show, that a 12% relative elongation is high, and many researchers desire to reach it by analyzing different approaches to additive manufacturing of products from titanium alloy. Thus, although the presence of the defective region does affect plastic strain, it does not lead to a significant reduction in the mechanical properties of the material. Consequently, if the requirements for the mechanical properties of a titanium product are satisfied regardless of the defective region, such a product can be put into operation. In this regard, the main factor that may limit the use of a part, is the wall thickness of the fabricated product. It is then necessary to provide a certain dimension tolerance of the as-built product geometry for its subsequent machining.

## CONCLUSIONS

This paper has clearly shown that uncontrolled wire fluctuations during the 3D printing process of titanium vertical walls resulted in the formation of defective regions in the structure. In these regions, the formation of the equiaxial grain structure was caused by violation of conditions of the non-stationary process of local metallurgy. In

contrast to the common structure represented by the coarse columnar grains of the β-phase, the average grain size in the defective region was 1.1 ± 0.3 mm. It was found that the phase composition in that region changed due to the presence of the reside β-phase alongside with α- and α′-phases throughout the wall height.

The identified structural changes did not affect the alloy microhardness. The average microhardness was 3.5 GPa in all the regions, which corresponded to the as-cast Ti-6Al-4V alloy hardness. The material properties under the static tension were more sensitive to the modified structure in the defective region. Thus, the specimens cut both in the deposition and growth directions demonstrated the UTS increase in the defective region and the decrease in the alloy plasticity. However, those changes were not critical, as even the small relative elongation of 12% met the requirements for commercial titanium Grade 2.

The defective region was characterized by the lower width of the EBAM vertical wall. Hence, provided that the material reached the required level of mechanical properties, the possibility of using the EBAM product was determined by a certain dimension tolerance of the as-built product geometry for its subsequent machining.

This work was carried out under the government contract No. III.23.2.11 in the Institute of Strength Physics and Materials Science SB RAS.

## REFERENCES

1. T. D. Ngo, A. Kashani, G. Imbalzano, *et al*., Compos. Part B-Eng., **143**, 172–196 (2018).
2. E. O. Olakanmi, R. F. Cochrane, and K. W. Dalgarno, Progr. Mater. Sci., **74**, 401–477 (2015).
3. D. Herzog, V. Seyda, E. Wycisk, and C. Emmelmann, Acta Mater., **117**, 371–392 (2016).
4. W. S.W. Harun, M. S. I. N. Kamariah, N. Muhamad, *et al*., Powder Technol., **327**, 128–151 (2018).
5. B. Wysocki, P. Maj, R. Sitek, *et al*., Appl. Sci., **7**, 657 (2017).
6. B. Wu, Z. Pan, D. Ding, *et al*., J. Mater. Process. Technol., **258**, 97–105 (2018).
7. L. Cordova, M. Campos, and T. Tinga, JOM, **71**, 1062–1072 (2019).
8. J. Fuchs, C. Schneider, and N. Enzinger, Weld. World, **62**, 267–275 (2018).
9. S. Yu. Tarasov, A. V. Filippov, N. N. Shamarin, *et al*., J. Alloys Compd., **803**, 364–370 (2019).
10. S.-H. Sun, Y. Koizumi, T. Saito, *et al*., Addit. Manuf., **23**, 457–470 (2018).
11. E. Brandl, A. Schoberth, and C. Leyens, Mat. Sci. Eng. A-Struct., **532**, 295–307 (2012).
12. J. Gockel, J. Beuth, and K. Taminger, Addit. Manuf., **1–4**, 119–126 (2014).
13. A. A. Shapiro, J. P. Borgonia, Q. N. Chen, *et al*., J. Spacecr. Rockets, **53**, 952–959 (2016).
14. P. Wanjara, K. Watanabe, C. Formanoir, de, *et al*., Adv. Mater. Sci. Eng., **2019**, 3979471 (2019).
15. K. S. Osipovich, A. V. Chumaevskii, A. A. Eliseev, *et al*., Russ. Phys. J., **62**, No. 8, 1486–1494 (2019).
16. Q. Wu, J. Lu, C. Liu, *et al*., Mater. Manuf. Process., **32**, 1881–1886 (2017).
17. F. Lia, J. Z. Park, J. S. Keist, *et al*., Mat. Sci. Eng. A-Struct., **717**, 1–10 (2018).
18. M. J. Bermingham, L. Nicastro, D. Kent, *et al*., J. Alloys Compd., **753**, 247–255 (2018).